Supplementary Materials for

Graphene Petal Foams with Hierarchical Micro- and Nano-Channels for Ultrafast Spontaneous and Continuous Oil Recovery

Shiwen Wu[1], Siyu Tian[1], Ruda Jian[1], Ting-Nan Wu[1], Tye David Milazzo[2],Tengfei Luo[2,*], Guoping Xiong[1,*]

[1.] Department of Mechanical Engineering, The University of Texas at Dallas, Richardson, Texas 75080, USA

[2.] Department of Aerospace and Mechanical Engineering, University of Notre Dame, Notre Dame, Indiana 46556, USA

* Corresponding authors: Tengfei Luo: tluo@nd.edu; Guoping Xiong: guoping.xiong@utdallas.edu

Section S1 Experimental Methods

S1.1 Chemicals and materials

Chemicals including type 2 oil, hydrochloric acid (37 wt.%), Methyl Methacrylate Polymer (PMMA), and ethyl lactate were purchased from Sigma-Aldrich. Other chemicals including mineral oil, methylene blue trihydrate, oil red O, and acetone (> 99.5%) were purchased from Thermo Fisher Scientific. Nickel foam (Purity > 99.99%, porosity > 95%) with a thickness of 1.6 mm and a surface density of 346 g m^{-2} was purchased from MTI Corporation. Teflon film with a thickness of around 80 μm was purchased from McMaster-Carr.

S1.2 Materials Fabrication

Fabrication of GPs/Ni. The GPs were synthesized by a customized inductively coupled plasma enhanced chemical vapor deposition (PECVD) system. In a typical procedure, a monolith of Ni foam substrate with a plane size of 1 cm × 10 cm was placed in a sealed cylindrical quartz tube, vacuumed to <10 Pa, and heated to 800 °C. A gas flow of CH_4 (6 mL min^{-1}) and H_2 (6 mL min^{-1}) was then injected into sealed tubes to act as precursors of GPs, with the growth pressure maintained at ~60 Pa. Subsequently, a radio frequency source of 300 W was coupled into the quartz tube. After growth for 2 h, the sample was cooled down under the protection of 20 mL min^{-1} Ar flow to obtain the GPs/Ni sample.

Fabrication of GPF film. The GPs/Ni samples were immersed in PMMA solution (4 wt.% in ethyl lactate), and then baked at 180 °C for 30 min. The PMMA-protected GPs/Ni samples were then immersed in a 3 M HCl solution at 80 °C overnight to completely dissolve the nickel ligaments to obtain GPF/PMMA composite. Finally, free-standing GPF samples were obtained by dissolving the PMMA with hot acetone at 50 °C for three times. The free-standing GPF was then protected by a thin Teflon film for further oil recovery tests.

S1.3 Materials Characterization

Scanning electron microscope (SUPRA40, Zeiss) was applied to characterize the morphology of the samples. An ultraviolet–visible–near-infrared spectrophotometer (Cary UV-Vis-NIR models 5000) with external diffuse reflectance accessories (DRA) 150 mm integrating sphere was used to measure the photonic transmittance (T) and reflectance (R). Photonic absorbance (A) was calculated by $A = 1 - T - R$. The oil recovery process is recovery by a digital camera. A solar simulator (Newport 94023) with a <3° collimated output was used as the light source. An optical filter was used to obtain a standard AM 1.5G spectrum. An optical power meter (S401C, Thorlabs) was used to detect the solar density. An infrared camera (A600, FLIR) was used to detect the surface temperature distribution of the GPF sample under solar irradiation of 1 kW m^{-2}. Oil viscosity was tested by a Discovery HR-2 hybrid rheometer from TA Instruments rigged with a DHR Jacket Peltier concentric cylinder and a TA Instrument Rotor conical/DIN SST Smart-Swap Bob (28.00 mm diameter). CANNON Instrument Company Standard S60 samples were employed calibrate the rheometer before conducting viscosity tests. All tests were conducted at ambient temperature of ~23 °C and atmospheric pressure of ~0.1 MPa, with a humidity of ~49%. Error analysis is conducted with multiple sets of repeatable tests.

Section S2 Supplementary Figures

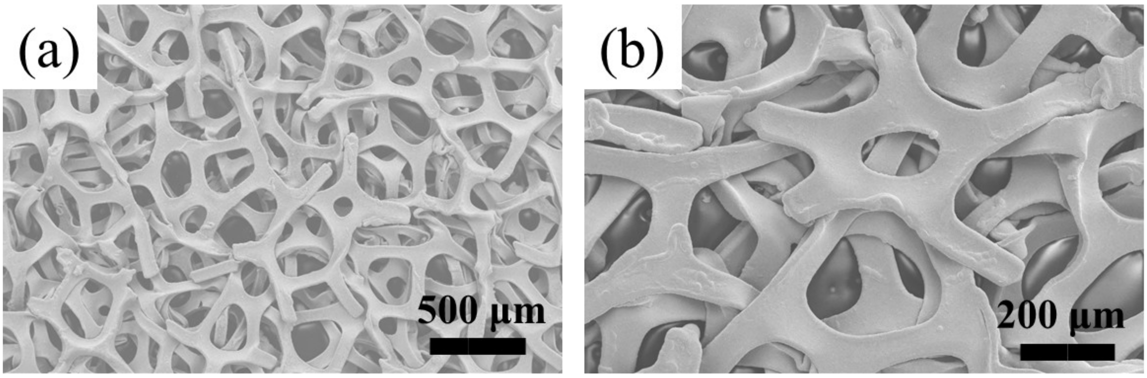

Figure S1. (a) and (b) SEM images of compressed Ni foam.

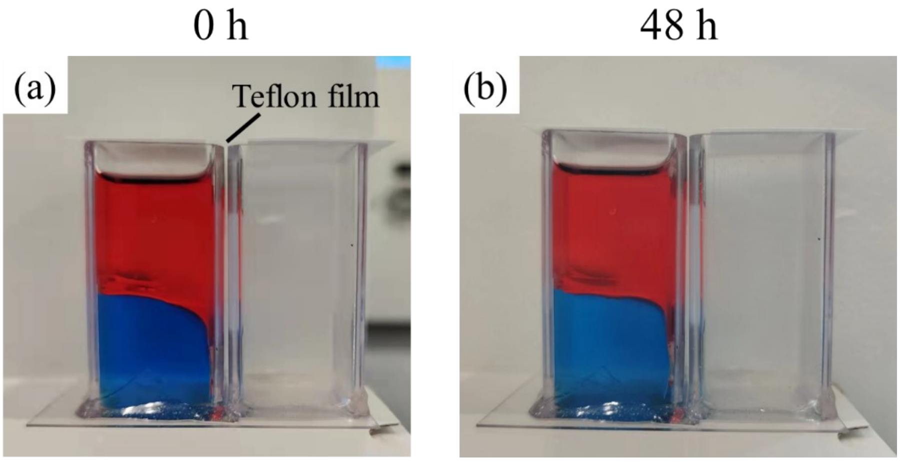

Figure S2. Optical images showing the oil recovery test by the Teflon substrate in dark condition at (a) 0 h and (b) 48 h. No oil is transferred from the left chamber to the right chamber during 48 h, indicating that the Teflon substrate exerts no influence on the oil recovery process.

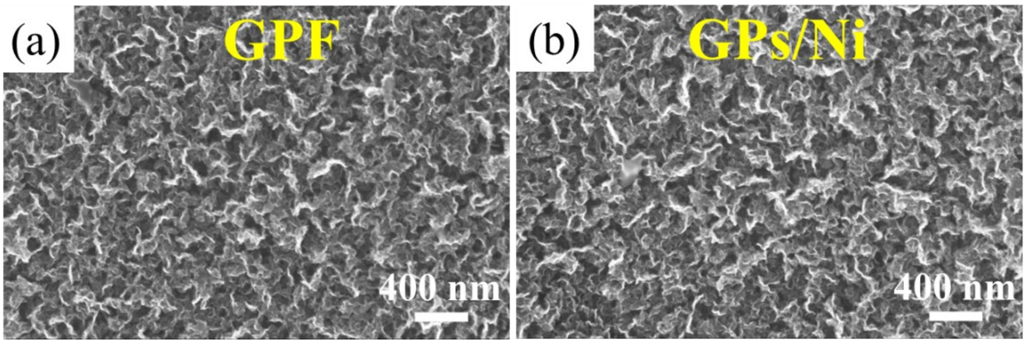

Figure S3. SEM images of (a) GPF and (b) GPs/Ni. GPs exhibit negligible structural changes during the etching of Ni foams.

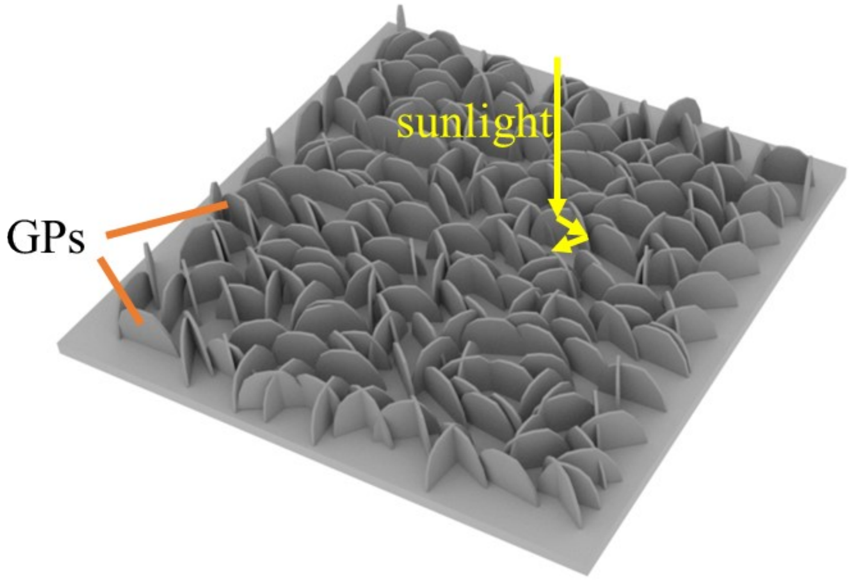

Figure S4. Schematic illustrating the light-trapped capability of GPs.

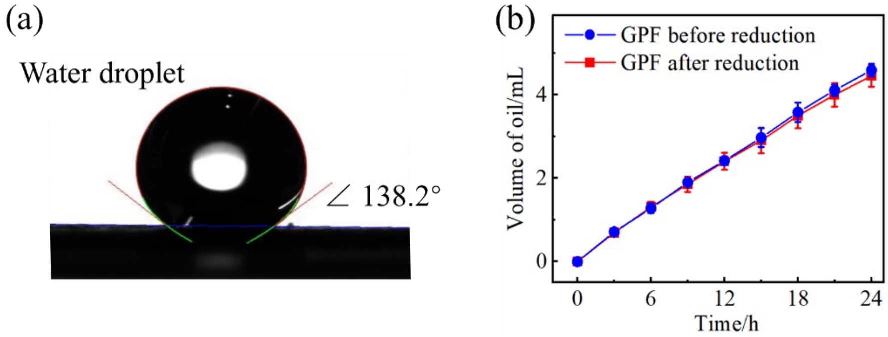

Figure S5. (a) Water contact angle measurement of the GPF skimmer after thermal reduction at 1000 °C in Ar environment for 2 h. (b) Volume evolutions of recovered oil by the GPF skimmers before and after the thermal reduction at 1 sun of solar illumination.

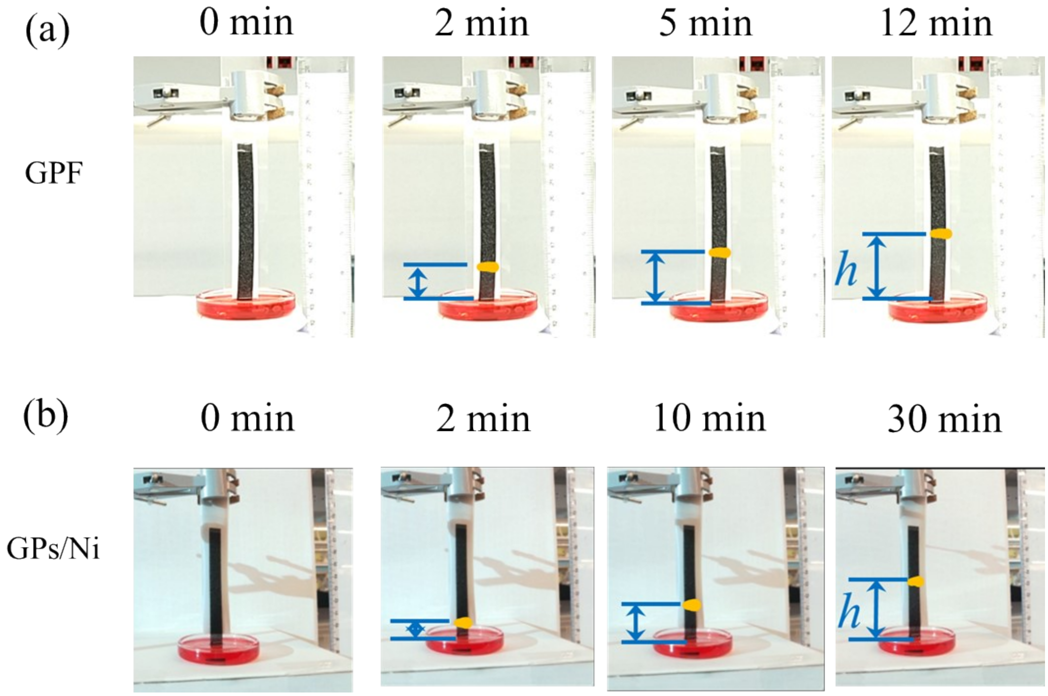

Figure S6. Optical images of capillary rise of the mineral oil against gravity on (a) GPF and (b) GPs/Ni oil skimmers. The red liquid is mineral oil dyed by oil red. The upper surfaces of the mineral oil are indicated by yellow lines. The capillary rises can be verified by Supplementary Videos S3-4.

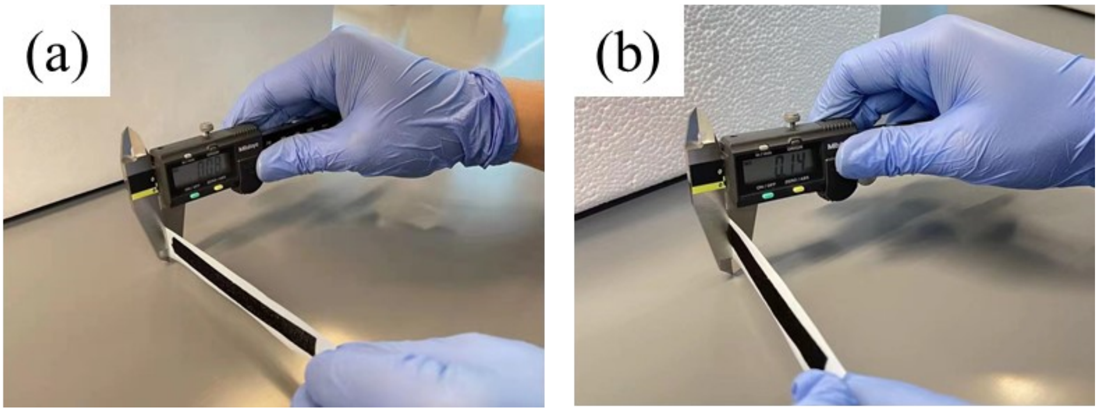

Figure S7. Optical images showing the thickness of GPF. (a) Thickness of GPF protected by a Teflon film. (b) Thickness of the Teflon film. Thickness of the GPF can thus be calculated by 0.14-0.08 mm = 0.06 mm.

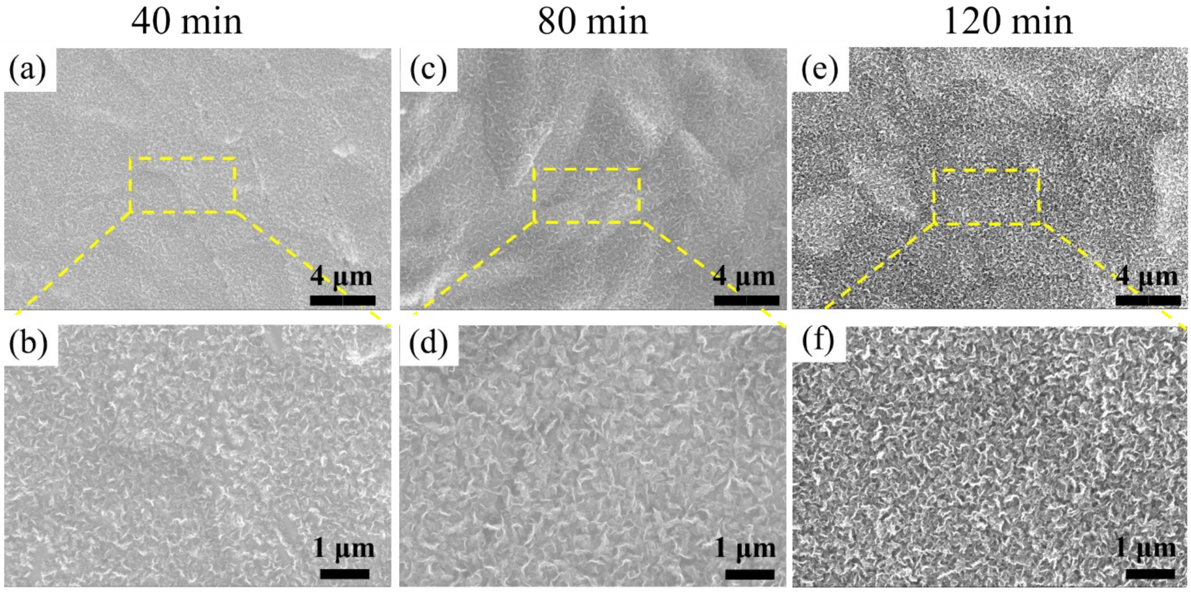

Figure S8. (a) and (b) SEM images of PECVD-grown GPF with a growth time of 40 min. (c) and (d) SEM images of GPF with a growth time of 80 min. (e) and (f) SEM images of GPF with a growth time of 120 min.

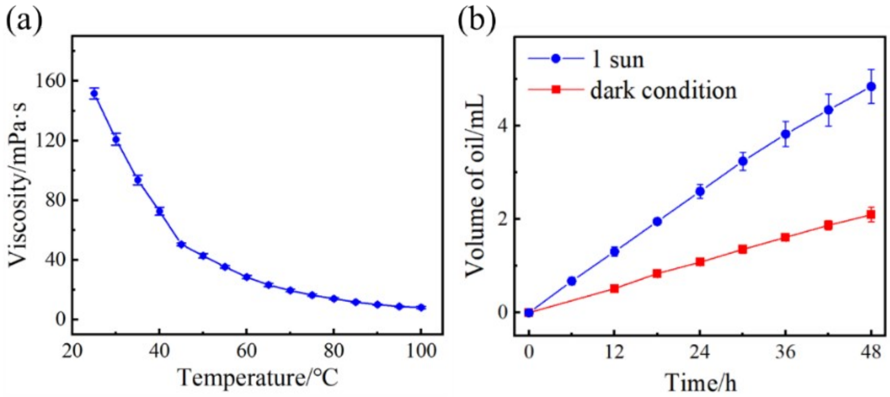

Figure S9. (a) Viscosity evolution of type 2 oil as a function of temperature. (b) Volume evolutions of recovered type 2 oil by the GPF skimmer at 1 sun and under dark condition.

Table S1 Comparison of oil recovery performance between the GPF oil skimmer and previous oil recovery devices

Year	External consuming energy	Solar irradiation	Oil recovery rate	Ref.
2016	Pump		580 L m^{-2} h^{-1}	1
2017	Pump and heater	-	672.8 kg m^{-2} h^{-1}	2
2018	Pump	-		3
2018	Pump	1.5 kW m^{-2}		4
2017	Squeezer and Heater	-		5
2017	Pump	-		6
2019	-	1 kW m^{-2}	123.3 L m^{-2} h^{-1}	7
2019	Pump	-		8
2019	Pump	1 kW m^{-2}	315 kg m^{-2} h^{-1}	9
2020	Squeezer	-		10
2020	Pump	1 kW m^{-2}	186.8 kg m^{-2} h^{-1}	11
2021	Pump and external alternating magnetic field	-	330.5 kg m^{-2} h^{-1}	12
2021	Pump	1 kW m^{-2}	124 kg m^{-2} h^{-1}	13
Our work	-	1 kW m^{-2}	318.8 L m^{-2} h^{-1}	-

References

(1) He, S.; Cheng, X.; Li, Z.; Shi, X.; Yang, H.; Zhang, H. Green and Facile Synthesis of Sponge-Reinforced Silica Aerogel and Its Pumping Application for Oil Absorption. *Journal of Materials Science* **2016**, *51* (3), 1292–1301. https://doi.org/10.1007/s10853-015-9427-9.

(2) Ge, J.; Shi, L.-A.; Wang, Y.-C.; Zhao, H.-Y.; Yao, H.-B.; Zhu, Y.-B.; Zhang, Y.; Zhu, H.-W.; Wu, H.-A.; Yu, S.-H. Joule-Heated Graphene-Wrapped Sponge Enables Fast Clean-up of Viscous Crude-Oil Spill. *Nature Nanotech* **2017**, *12* (5), 434–440. https://doi.org/10.1038/nnano.2017.33.

(3) Wang, X.; Pan, Y.; Shen, C.; Liu, C.; Liu, X. Facile Thermally Impacted Water-Induced Phase Separation Approach for the Fabrication of Skin-Free Thermoplastic Polyurethane Foam and Its Recyclable Counterpart for Oil–Water Separation. *Macromolecular Rapid Communications* **2018**, *39* (23), 1800635. https://doi.org/10.1002/marc.201800635.

(4) Zhang, C.; Wu, M.-B.; Wu, B.-H.; Yang, J.; Xu, Z.-K. Solar-Driven Self-Heating Sponges for Highly Efficient Crude Oil Spill Remediation. *Journal of Materials Chemistry A* **2018**, *6* (19), 8880–8885. https://doi.org/10.1039/C8TA02336K.

(5) Liu, Y.; Shi, Q.; Hou, C.; Zhang, Q.; Li, Y.; Wang, H. Versatile Mechanically Strong and Highly Conductive Chemically Converted Graphene Aerogels. *Carbon* **2017**, *125*, 352–359. https://doi.org/10.1016/j.carbon.2017.09.072.

(6) Wang, Y.; Liu, X.; Lian, M.; Zheng, G.; Dai, K.; Guo, Z.; Liu, C.; Shen, C. Continuous Fabrication of Polymer Microfiber Bundles with Interconnected Microchannels for Oil/Water Separation. *Applied Materials Today* **2017**, *9*, 77–81. https://doi.org/10.1016/j.apmt.2017.05.007.

(7) Wu, S.; Yang, H.; Xiong, G.; Tian, Y.; Gong, B.; Luo, T.; Fisher, T. S.; Yan, J.; Cen, K.; Bo, Z.; Ostrikov, K. K. Spill-SOS: Self-Pumping Siphon-Capillary Oil Recovery. *ACS Nano* **2019**, *13* (11), 13027–13036. https://doi.org/10.1021/acsnano.9b05703.

(8) Xu, Z.; Wang, J.; Li, H.; Wang, Y. Coating Sponge with Multifunctional and Porous Metal-Organic Framework for Oil Spill Remediation. *Chemical Engineering Journal* **2019**, *370*, 1181–1187. https://doi.org/10.1016/j.cej.2019.03.288.

(9) Wang, Y.; Zhou, L.; Luo, X.; Zhang, Y.; Sun, J.; Ning, X.; Yuan, Y. Solar-Heated Graphene Sponge for High-Efficiency Clean-up of Viscous Crude Oil Spill. *Journal of Cleaner Production* **2019**, *230*, 995–1002. https://doi.org/10.1016/j.jclepro.2019.05.178.

(10) Peptide-Based Gel in Environmental Remediation: Removal of Toxic Organic Dyes and Hazardous Pb2+ and Cd2+ Ions from Wastewater and Oil Spill Recovery | Langmuir https://pubs.acs.org/doi/abs/10.1021/acs.langmuir.0c02205 (accessed 2021 -12 -08).

(11) Li, Q.; Sun, Q.; Li, Y.; Wu, T.; Li, S.; Zhang, H.; Huang, F. Solar-Heating Crassula Perforata-Structured Superoleophilic CuO@CuS/PDMS Nanowire Arrays on Copper Foam for Fast Remediation of Viscous Crude Oil Spill. *ACS Appl. Mater. Interfaces* **2020**, *12* (17), 19476–19482. https://doi.org/10.1021/acsami.0c01207.

(12) Song, Y.; Shi, L.-A.; Xing, H.; Jiang, K.; Ge, J.; Dong, L.; Lu, Y.; Yu, S.-H. A Magneto-Heated Ferrimagnetic Sponge for Continuous Recovery of Viscous Crude Oil. *Advanced Materials* **2021**, *33* (36), 2100074. https://doi.org/10.1002/adma.202100074.

(13) Wu, X.; Lei, Y.; Li, S.; Huang, J.; Teng, L.; Chen, Z.; Lai, Y. Photothermal and Joule

Heating-Assisted Thermal Management Sponge for Efficient Cleanup of Highly Viscous Crude Oil. *Journal of Hazardous Materials* **2021**, *403*, 124090. https://doi.org/10.1016/j.jhazmat.2020.124090.